

# Description of Induced Nuclear Fission with Skyrme Energy Functionals: II. Finite Temperature Effects

N. Schunck,<sup>1</sup> D. Duke,<sup>2</sup> and H. Carr<sup>2</sup>

<sup>1</sup>*Physics Division, Lawrence Livermore National Laboratory, Livermore, CA 94551, USA*

<sup>2</sup>*School of Computing, University of Leeds, UK*

(Dated: July 30, 2021)

Understanding the mechanisms of induced nuclear fission for a broad range of neutron energies could help resolve fundamental science issues, such as the formation of elements in the universe, but could have also a large impact on societal applications in energy production or nuclear waste management. The goal of this paper is to set up the foundations of a microscopic theory to study the static aspects of induced fission as a function of the excitation energy of the incident neutron, from thermal to fast neutrons. To account for the high excitation energy of the compound nucleus, we employ a statistical approach based on finite-temperature nuclear density functional theory with Skyrme energy densities, which we benchmark on the  $^{239}\text{Pu}(n,f)$  reaction. We compute the evolution of the least-energy fission pathway across multidimensional potential energy surfaces with up to five collective variables as a function of the nuclear temperature, and predict the evolution of both the inner and outer fission barriers as a function of the excitation energy of the compound nucleus. We show that the coupling to the continuum induced by the finite temperature is negligible in the range of neutron energies relevant for many applications of neutron-induced fission. We prove that the concept of quantum localization introduced recently can be extended to  $T > 0$ , and we apply the method to study the interaction energy and total kinetic energy of fission fragments as a function of the temperature for the most probable fission. While large uncertainties in theoretical modeling remain, we conclude that finite-temperature nuclear density functional may provide a useful framework to obtain accurate predictions of fission fragment properties.

PACS numbers: 21.60.Jz, 24.75.+i, 25.85.Ec, 27.90.+b

## I. INTRODUCTION

One of the most important challenges for a theory of induced fission is the capability to predict the evolution of observables such as the charge, mass, relative yields, total kinetic energy, total excitation energy, and decay patterns of fission fragments as a function of the energy of the incident neutron. Recall that the energy of neutrons produced in induced fission follows roughly a Maxwellian distribution, and the energy range of interest for applications is typically comprised between a few eV and up to about 14 MeV [1, 2]. Following an original idea by Bohr and Wheeler, induced fission is modeled as the break-up of the compound nucleus formed by absorption of the incident neutron [3]. In this picture, neutron kinetic energies of the order of the MeV correspond to very high excitation energies of the compound nucleus, where the nuclear level density is very large [4].

In a density functional theory (DFT) approach to induced fission, one may be tempted to describe such highly excited states directly, via various general schemes such as the random phase approximation or the generator coordinate method. However, even assuming all of these methods were properly defined for the kind of energy densities used in practice (cf. the discussions about multi-reference density functional theory in Refs. [5–9]), the very large density of states to consider may jeopardize the success of such a strategy. In addition, it is expected that dissipation plays a role in fission, and extensions of these methods to account for explicit couplings between

collective and intrinsic degrees of freedom have only recently been outlined [10].

In this context, the finite-temperature formulation of the nuclear density functional theory provides an appealing alternative [11–14]. Assuming that the system is described by a mixed quantum state uniquely determined by the form of the statistical density operator provides a convenient basis to quantify the impact of excitation energy on the deformation properties of the compound nucleus.

There have been many applications of the finite-temperature formalism in nuclear structure, including early studies of fission barriers using the Thomas-Fermi approximation [15–20], the Hartree-Fock (FT-HF) approximation [21, 22], and more recently at the Hartree-Fock-Bogoliubov (FT-HFB) approximation [23–25], or applications in the calculation of Giant Dipole Resonances and level densities [26–29]. Until now, however, there has been no systematic study of the validity and applicability of finite-temperature DFT in the description of induced fission. Of particular importance are the evolution of scission configurations and of fission fragment properties as a function of the excitation energy of the compound nucleus.

In a previous paper, thereafter referred to as (I), we have used the nuclear DFT with Skyrme energy densities to analyze static properties of the neutron-induced fission of the  $^{239}\text{Pu}$  nucleus [30]. In particular, we have discussed the role of triaxiality at scission, the dependence on the parametrization of the energy density functional (EDF) –

including the pairing channel, and the critical importance of scission configurations. The topological method that we have proposed to identify the latter allows to define a region in the collective space where scission should take place. We have then shown that localization techniques borrowed from electronic structure theory can allow us to approach the asymptotic conditions of two independent fission fragments. This is key to extracting theoretically sound estimates of the total excitation energy of the fragments.

Building on this previous study, the goals of this second paper are, therefore, (i) to establish and validate the framework for nuclear DFT calculations at finite temperature in the specific context of induced fission, (ii) to study the evolution of fission barriers and the position and nature of scission configurations as functions of the excitation energy of the incident neutron, and (iii) to explore the consequences of the finite-temperature description for the determination of fission fragment properties. This paper is the second in a series of several articles focusing on the microscopic description of induced fission within the framework of the nuclear density functional theory with Skyrme energy densities.

Section II contains a brief reminder of the theoretical framework, from basic definitions and concepts related to neutron-induced nuclear fission to the extension of nuclear density functional theory at finite temperature with Skyrme functionals. Section III focuses on the evolution of potential energy surfaces and fission barriers with temperature. Section IV is devoted to fission fragment properties at finite temperature, including the extension of the concept of quantum localization, a study of the coupling to the continuum, and an estimate of the nuclear and Coulomb interaction energy of the fission fragments.

## II. THEORETICAL FRAMEWORK

Our theoretical approach is based on the local density approximation of the energy density functional (EDF) theory of nuclear structure. We recall in the next few sections some of the basic ingredients of the EDF theory pertaining to the description of induced nuclear fission at given excitation energy.

### A. Thermodynamical and Statistical View of Neutron-Induced Fission

We begin by recalling a few well-known facts about neutron-induced fission in order to avoid confusions about the vocabulary used in this work. For fissile elements such as  $^{239}\text{Pu}$ , the capture of a thermal neutron (in equilibrium with the environment and with an average kinetic energy of the order of  $E_n \approx 0.02$  eV) is sufficient to induce fission. The energy balance of the reaction is such that the compound nucleus  $(Z, N)$  formed after the neutron has been captured is at an excitation energy

equal to  $|S(N)|$ , where  $S(N)$  is the one-neutron separation energy. In fissile elements, this quantity is larger than the fission barrier height, leading to fission. Note that the concept of nuclear deformation, hence of potential energy surfaces (PES) and fission barriers, is highly model-dependent: it is rooted in the mean-field approach to nuclear structure, and originates from the spontaneous symmetry breaking of rotational invariance in the intrinsic frame of the nucleus [31, 32]. However, the success of macroscopic-microscopic and self-consistent approaches in describing both qualitatively and quantitatively the main features of the fission process is evidence that such a concept is very useful in practice.

#### 1. Statistical Description of the Compound Nucleus

In a microscopic theory of fission based on nuclear DFT, it is assumed that the fission process is driven by a small set of collective degrees of freedom  $\mathbf{q}$ . It is further assumed that the potential energy surface of the compound nucleus in this collective space can be reliably described at the Hartree-Fock-Bogoliubov (HFB) approximation. This implies that the collective variables are defined as expectation values of specific operators, such as, e.g., multipole moments, on the HFB vacuum. The PES is then generated by performing a series of constrained HFB calculations. Such an approach is clearly an approximation, since the HFB vacuum is the lowest energy state for the set of constraints  $\mathbf{q}$  while the compound nucleus is, by definition, in an excited state. Nonetheless, early calculations of fission fragment charge mass yields and total kinetic energy for low-energy neutron-induced fission obtained within this approximation give a reasonably good agreement with experimental data [33–35]. In fact, a similar approximation is implicitly made in macroscopic-microscopic methods, with a similarly good reproduction of experimental data [36, 37].

If the energy of the incident neutron  $E_n$  increases (fast neutrons), the excitation energy  $E^*$  of the compound nucleus increases accordingly. For  $E_n \approx 14$  MeV,  $E^*$  can be typically of the order of 20 MeV or more in actinides. In this regime, the nuclear level density is very large, of the order of  $\rho(E^*) \approx 10^{12}$  MeV $^{-1}$  at  $E^* \approx 20$  MeV and growing exponentially with  $E^*$ , see, e.g., Ref. [26]. It thus becomes more and more unlikely that constrained HFB vacua can still provide a realistic description of the nuclear potential energy surface, and more generally of the fission process. In addition, the extremely large level density suggests that direct calculation of excited states could prove extremely challenging. Instead, we will seek to describe induced fission with finite-temperature density functional theory (FT-DFT).

In this work, we neglect particle evaporation or gamma emission. In other words, we do not consider second chance fission – the fission of the nucleus after one neutron has been emitted, or third chance fission – after two neutrons have been emitted. Therefore, the com-

pound nucleus is viewed as a closed and isolated system. In statistical physics, such systems should be treated in the microcanonical ensemble [38]. However, counting the number  $\mathcal{N}(E^*)$  of microstates of the system at any given experimental excitation energy  $E^*$  would require one to have access to the full eigen-spectrum of the nucleus. In practice, this is impossible and the microcanonical treatment of the problem must be ruled out [29].

In nuclear DFT, the nuclear wave-function takes the form of a HFB vacuum: it is not an eigenfunction of the nuclear Hamiltonian, nor of the particle number operator. This implies that the total energy and the number of particles in the system are only known on average: there can be fluctuations of both quantities, of either quantum or/and statistical origin [29]. This observation suggests to use the grand canonical ensemble to describe the nuclear system. The density operator  $\hat{D}$  characterizing such an ensemble is obtained by maximizing Gibbs entropy under the constraints that the energy and particle numbers are constant on average. The resulting equation is equivalent to expressing the thermodynamical grand potential  $\Omega$  at constant temperature  $T$  and chemical potential  $\lambda$  in terms of the grand partition function. The relevant thermodynamic potential is then the Helmholtz free energy  $F$  [38]. Note that, in this statistical setting, the temperature  $T$  is, *stricto sensu*, only a Lagrange parameter used to maintain the energy constant on average.

## 2. Neutron Incident Energy and Nuclear Temperature

One of the difficulties in the FT-DFT description of fission is to interpret the temperature introduced in the theory, in particular in terms of the excitation energy of the compound nucleus. It was suggested in Refs. [39, 40] that the temperature  $T$  be determined locally at every point in the collective space by assuming that all the excitation energy at deformation  $\mathbf{q}$  is entirely of thermal nature. In practice, this scenario has only been applied in the macroscopic-microscopic approach to nuclear structure. Starting from the total energy at  $T = 0$  expressed as the sum of a macroscopic term, a shell correction and a pairing correction, one determines the local temperature  $T(\mathbf{q})$  given the experimental excitation energy  $E^*$ ; this temperature is then used to generate a new, temperature-dependent, PES where shell and pairing corrections are locally damped. This procedure has been used to describe superdeformed bands at high-spin and high excitation energy [41], hyperdeformation and the Jacobi shape transition [42] and the dynamics of induced fission [43].

The feasibility of such an approach, however, is entirely contingent on the assumed decomposition of the energy into a temperature-independent part (the liquid drop energy) and a temperature-dependent microscopic correction, both of which depend on deformation. In FT-DFT, such a decomposition does not exist. All of the total energy is a function of the temperature: if one followed the recipe of selecting at point  $\mathbf{q}$  in the collective space the

DFT solution at  $T = T(\mathbf{q})$  such that  $E(\mathbf{q}) = E^*$ , the total energy of the nucleus would become, by construction, constant across the collective space, and the very concept of a PES with barriers and valleys would be lost.

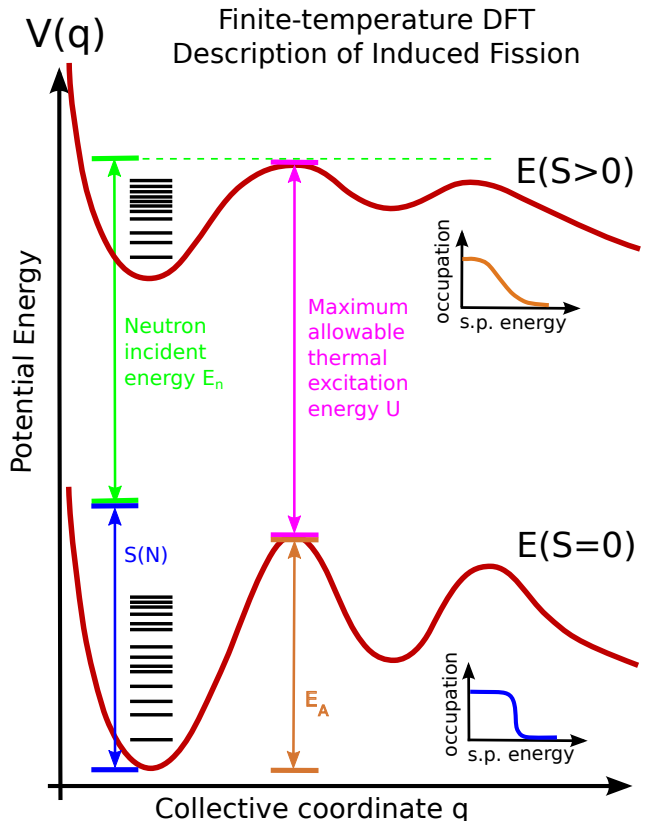


FIG. 1. (color online) Schematic illustration of how induced fission is described within density functional theory at finite temperature. The separation energy of the compound nucleus  $(Z, N)$  is denoted  $S(N)$ .

In order to retain the view of fission as a large amplitude collective motion through a PES while simultaneously accounting for the effect of excitation energy via FT-DFT, we are thus bound to make the additional assumption that the temperature must be constant across the PES. More specifically, the potential energy surface can be defined either as the function  $F(\mathbf{q}; T)$ , where  $F$  is the Helmholtz free energy, or by the function  $E(\mathbf{q}; S)$ , where  $S$  is the entropy; see Sec. III A for additional details. In addition, since fission occurs for all neutron energies of interest, we will assume that the total excitation energy  $E^*$  of the compound nucleus must be higher than the top of the barrier computed at  $S > 0$ : this requirement gives us the maximum allowable *thermal* excitation energy  $U$  available to the system. Figure 1 illustrates how this works in practice: the thermal excitation energy is related to the entropy  $S$  of the FT-HFB theory through  $E_n + S(N) = U(S) + E_A$ , where  $E_n$  is the kinetic energy of the incident neutron,  $S(N)$  is the one-neutron separation energy of the compound nucleus, and  $E_A$  is

the height of the first fission barrier at  $S = 0$ . In calculations with energy functionals, the height of the first fission barrier may be larger than the separation energy,  $E_A > S(N)$ , which would contradict the experimental observation that the nucleus is fissile. For example, for  $^{240}\text{Pu}$ , we find  $S(N) = 7.09$  MeV and  $E_A = 7.65$  MeV. In order to guarantee that thermal neutrons trigger fission, we thus have to introduce a small offset  $\delta = E_A - S(N)$  such that  $E_n + S(N) + \delta = U(S) + E_A$ . In this particular case,  $U(S) = E_n$ . Note that this offset is a purely empirical correction needed to guarantee the fissile nature of the compound nucleus.

To finish this section, we note that the most rigorous way to combine a statistical description of the compound nucleus at high excitation energy with the conventional view of fission as a large amplitude collective motion would be to use the Liouville equation for the grand canonical density operator. Starting from some initial condition  $\hat{D}_0$ , the Liouville equation gives the time-evolution of  $\hat{D}$ . A collective, time-dependent equation of motion for the nucleus could then be obtained, at least in principle, by introducing the HFB approximation for the density operator and a small set of collective variables that would carry the time-dependence. Such a procedure was outlined in a recent paper, but numerous challenges remain to implement it in practice [44].

## B. Finite Temperature HFB Theory

As recalled above, we use the finite-temperature HFB theory to describe the compound nucleus at given excitation energy. The FT-HFB theory has a long history in the literature [13, 14, 27, 28, 45–48]. Here, we only recall the physical assumptions that are most relevant to this work. The compound nucleus is assumed to be in a state of thermal equilibrium at temperature  $T$ . In the grand canonical ensemble, the system is then characterized by the statistical density operator  $\hat{D}$ ,

$$\hat{D} = \frac{1}{Z} e^{-\beta(\hat{H} - \lambda\hat{N})}, \quad (1)$$

where  $Z$  is the grand partition function,  $\beta = 1/kT$ ,  $\hat{H}$  is the Hamiltonian of the system,  $\lambda$  the Fermi level and  $\hat{N}$  the number operator [13, 38]. In this work, the Hamiltonian is a two-body effective Hamiltonian with the Skyrme pseudopotential. The statistical average  $\langle \hat{F} \rangle$  of an operator  $\hat{F}$  is defined as

$$\langle \hat{F} \rangle = \text{Tr} [\hat{D}\hat{F}], \quad (2)$$

where the trace can be computed in any convenient basis of the Fock space, i.e., it involves many-body states.

In the mean-field approximation of the density operator, the real Hamiltonian  $\hat{H}$  is replaced by a quadratic form  $\hat{K}$  of the particle operators [13, 27, 28, 48]. Given a generic basis  $|i\rangle$  of the single-particle space, with  $c_i$

and  $c_i^\dagger$  the corresponding single-particle operators, this is expressed by

$$\hat{K} = \sum_{ij} K_{ij} c_i^\dagger c_j \quad (\text{HF}), \quad (3)$$

$$\hat{K} = \frac{1}{2} \sum_{ij} K_{ij}^{11} c_i^\dagger c_j + \frac{1}{2} \sum_{ij} K_{ij}^{22} c_i c_j^\dagger + \frac{1}{2} \sum_{ij} K_{ij}^{20} c_i^\dagger c_j^\dagger + \frac{1}{2} \sum_{ij} K_{ij}^{02} c_i c_j \quad (\text{HFB}), \quad (4)$$

where HF refers to the Hartree-Fock approximation of the partition function, and HFB to the Hartree-Fock-Bogoliubov approximation. As a consequence of the Wick theorem for ensemble averages, there is a one-to-one correspondence between the one-body density matrix  $\hat{\rho}$  (HF) or generalized density matrix  $\hat{\mathcal{R}}$  (HFB) and the operator  $\hat{K}$  [13, 28]. In particular: all statistical traces can be computed by taking the trace in the single-particle space [13],

$$\langle \hat{F} \rangle = \text{Tr} [\hat{D}\hat{F}] = \begin{cases} \text{tr} [\hat{\rho}\hat{F}], & (\text{HF}), \\ \frac{1}{2} \text{tr} [\hat{\mathcal{R}}\hat{F}], & (\text{HFB}). \end{cases} \quad (5)$$

The forms (3)-(4) of the operator  $\hat{K}$  defining the statistical density operator are generic. The matrix elements of  $\hat{K}$  are thus taken as variational parameters and determined by requesting that the grand potential be minimum with respect to variations  $\delta\hat{K}$ . This leads to the identification  $\hat{K} = \hat{h}$  (HF) and  $\hat{K} = \hat{\mathcal{R}}$  (HFB), that is

$$\hat{\rho} = \frac{1}{1 + \exp(\beta\hat{h})}, \quad (\text{HF}), \quad (6)$$

$$\hat{\mathcal{R}} = \frac{1}{1 + \exp(\beta\hat{\mathcal{H}})}, \quad (\text{HFB}), \quad (7)$$

where  $\hat{h}$  is the usual HF Hamiltonian,  $\hat{\mathcal{H}}$  the HFB Hamiltonian and  $\beta = 1/kT$ . These equations are the HF and HFB equations; see [13, 28] for the demonstration. Note that the variational principle does not require that either of these matrices be diagonalized. In practice, building the density matrix (generalized density) from the eigenvectors of  $h$  ( $\mathcal{R}$ ) just happens to be a very convenient way to guarantee that the functional equations (6)-(7) are satisfied.

In the basis where  $\mathcal{H}$  is diagonal, one easily shows that the statistical occupation of a one quasi-particle state reads

$$\text{Tr} [\hat{D}\beta_\mu^\dagger\beta_\mu] = \frac{1}{1 + e^{\beta E_\mu}} \delta_{\mu\nu} = f_{\mu\nu} \delta_{\mu\nu}, \quad (8)$$

with  $E_\mu$  the q.p. energy, i.e., the eigenvalue of  $\mathcal{H}$ . This result allows to show that the matrix of the one-body density matrix and pairing tensor in the s.p. basis are modified according to

$$\rho_{ij} = \text{Tr} [\hat{D}c_j^\dagger c_i] = (V^*(1-f)V^T)_{ij} + (UfU^\dagger)_{ij}, \quad (9)$$

$$\kappa_{ij} = \text{Tr} [\hat{D}c_j c_i] = (V^*(1-f)U^T)_{ij} + (UfV^\dagger)_{ij} \quad (10)$$

where the  $U$  and  $V$  are the matrices of the Bogoliubov transformation.

The finite-temperature extension of the HFB theory poses two difficulties. First, we recall that, in the HFB theory at zero temperature, the component  $V_\mu$  of the q.p.  $\mu$  is always localized for a system with negative Fermi energy  $\lambda < 0$  [49, 50]. The consequence is that both the mean-field, the pairing field, and the expectation value of any physical observable  $\hat{O}$  are also localized (since  $\rho = V^*V^T$  and  $O = \text{tr}\hat{O}\hat{\rho}$ ). However, at finite-temperature, we note that, even though the pairing tensor remains always localized for  $\lambda < 0$ , the density matrix does not. More specifically, all q.p.  $\mu$  with  $0 < E_\mu < -\lambda$  give a localized contribution to the mean-field and physical observables, while all q.p. with  $E_\mu > -\lambda$  yield a coupling with the continuum through the  $(UfU^\dagger)$  term of the density matrix, see Sec. IV D for more details. The existence of this coupling was already pointed out and quantified in the context of the Hartree-Fock theory at finite temperature [22, 51, 52].

The second difficulty is that, in the statistical description of the system by a grand canonical ensemble, only the average value of the energy and the particle number (and any other constrained observables) are fixed. In addition to the quantum fluctuations brought about by the fact that DFT wave-functions are not eigenstates of the Hamiltonian, thermal (or statistical) fluctuations are also present [29]. They increase with temperature and should decrease with the system size [38]. From a statistical point of view, the FT-HFB theory only gives the most probable solution within the grand-canonical ensemble, the one that corresponds to the lowest free energy. Mean values and deviations around the mean values of any observable  $\hat{O}$  can be computed in the classical limit as in Ref. [48]

$$\bar{O} = \frac{\int d^N \mathbf{q} \mathcal{O}(\mathbf{q}) e^{-\beta F(T, \mathbf{q})}}{\int d^N \mathbf{q} e^{-\beta F(T, \mathbf{q})}}. \quad (11)$$

Such integrals should in principle be computed across the whole collective space defined by the variables  $\mathbf{q} = (q_1, \dots, q_N)$  and require the knowledge of the volume element  $d^N \mathbf{q}$ . Other possibilities involve functional integral methods [53]. In this work, we only consider the most probable value for observables and disregard all statistical fluctuations.

### C. Skyrme EDF and Numerical and Numerical Implementation

We briefly recall that we work with Skyrme energy densities, for which the energy of the nucleus is a functional of the one-body density matrix. In this paper, all calculations have been performed at the FT-HFB level with the SkM\* parametrization of the Skyrme pseudopotential

[54]. The pairing functional originates from a density-dependent, mixed surface-volume pairing force. In the calculations of the densities, all quasi-particles above a cut-off energy  $E_{\text{cut}} = 60$  MeV are dismissed. The pairing strength for both the proton and neutron force were fitted locally on the 3-point formula of the odd-even mass difference in  $^{240}\text{Pu}$ , see (I) for details. Contrary to (I), the UNEDF family of functionals was not considered here, since they require the Lipkin-Nogami prescription, which is not available yet at finite temperature.

As in (I), the nuclear shape is characterized by a set  $\mathbf{q} = (q_1, \dots, q_N)$  of  $N$  collective variables. In this work, we consider the expectation value  $q_{\lambda\mu}$  of the multipole moment operators  $\hat{Q}_{\lambda\mu}$  on the HFB vacuum for the: axial quadrupole  $(\lambda, \mu) = (2, 0)$ ; triaxial quadrupole  $(\lambda, \mu) = (2, 2)$ ; axial octupole  $(\lambda, \mu) = (3, 0)$  and axial hexadecapole  $(\lambda, \mu) = (4, 0)$ . We also employ the expectation value of the neck operator  $\hat{Q}_N$  with the range  $a_N = 1.0$  fm. The finite-temperature extension of the Wick theorem guarantees that the expectation value of these (one-body) operators at  $T > 0$  take the same form as at  $T = 0$ , only with the density matrix computed as in (9). Constrained HFB solutions are obtained by using a variant of the linear constraint method where the Lagrange parameter is updated based on the cranking approximation of the random phase approximation (RPA) matrix [55–57]. This method has been extended to handle non-zero temperatures. All calculations were performed with the DFT solvers HFODD [57] and HF-BTHO [58]. In both codes, the HFB eigenfunctions are expanded on a one-center harmonic oscillator (HO) basis. In all calculations reported here, this expansion was based on the lowest  $N_{\text{states}} = 1100$  states of the deformed HO basis. The largest oscillator shell entering the expansion was  $N_{\text{max}} = 31$ . The deformation  $\beta_2$  and the oscillator frequency  $\omega_0$  of the HO were parametrized empirically as a function of the requested expectation value  $q_{20}$  of the quadrupole moment  $\hat{Q}_{20}$  according to

$$\omega_0 = \begin{cases} 0.1 \times q_{20} e^{-0.02 q_{20}} + 6.5 \text{MeV} & \text{if } |q_{20}| \leq 30b \\ 8.14 \text{MeV} & \text{if } |q_{20}| > 30b \end{cases} \quad (12)$$

and

$$\beta = 0.05 \sqrt{q_{20}} \quad (13)$$

We refer the reader to (I) and Ref. [59] for further details on the convergence properties of the basis.

### III. EVOLUTION OF DEFORMATION PROPERTIES AT FINITE TEMPERATURE

In this section, we illustrate the modifications of the collective potential energy surfaces discussed in (I) induced by the finite temperature. In particular, we give an accurate estimate of the evolution of fission barrier heights as a function of the excitation energy of the compound nucleus formed in the reaction  $^{239}\text{Pu}(n, f)$ .

### A. Fission Pathway of Least Energy

As recalled in Sec. IIB the FT-HFB theory is built on the grand-canonical description of the nucleus as a system in thermal equilibrium maintained at constant temperature  $T$ . Since particle number is constant on average across the whole collective space, the thermodynamical potential relevant to study deformation effects is the Helmholtz free energy  $F = E - TS$ , which is computed at constant volume  $V$  and temperature  $T$ . The potential energy surface is characterized by the ensemble of points  $F(\mathbf{q})$ , and variations of free energy between two points  $\mathbf{q}_1$  and  $\mathbf{q}_2$  are computed through  $\delta F|_T = F(\mathbf{q}_1, T) - F(\mathbf{q}_2, T)$ .

We show in Fig. 2 the free energy of the compound nucleus  $^{240}\text{Pu}$  along the least-energy fission pathway for temperatures ranging between 0 and 1.75 MeV by steps of 250 keV. Based on the discussion of Sec. IIA, this corresponds to maximal excitation energies of about  $E^* \approx 80$  MeV for the compound nucleus. Recall that the height of the first fission barrier is  $E_A = 7.65$  MeV in  $^{240}\text{Pu}$  for the SkM\* functional; this corresponds to maximum neutron kinetic energies of about  $E_n \approx 73$  MeV. The least-energy fission pathway is found according to the procedure presented in (I): while the value of the axial quadrupole moment is constrained, the triaxial, octupole and hexadecapole moments are unconstrained, so that triaxiality and mass asymmetry effects are taken into account.

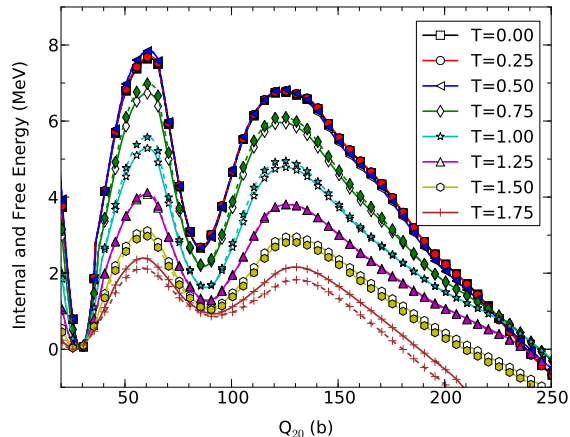


FIG. 2. (color online) Plain lines with open symbols: Free energy along the least-energy fission pathway in  $^{240}\text{Pu}$  for finite temperatures  $T = 0.00, \dots, 1.75$  MeV. Dashed lines with plain symbols: Corresponding internal energy  $E$  at constant entropy  $S$ . All curves are normalized to their ground-state value. Temperature units are in MeV.

It has been argued in the literature that an isentropic description of fission should be preferred over the isothermal description [20, 25]. In this representation, the thermodynamical potential is the internal energy  $E$ , which is computed at constant volume  $V$  and entropy  $S$ . The

potential energy surface is now the ensemble of points  $E(\mathbf{q})$ , and variations of energy are computed through  $\delta E|_S = E(\mathbf{q}_1; S) - E(\mathbf{q}_2; S)$ . The Maxwell relations of thermodynamics state that the variations of the free energy  $\delta F|_T$  over some extensive state variable  $X$  (at constant temperature) are equal to the variations of the internal energy  $\delta E|_S$  (at constant entropy) [38].

Figure 2 also shows the internal energy  $E(\mathbf{q}; S)$  at constant entropy deduced from the free energy curves: At each value  $\mathbf{q}$  of the constrained collective variable (here, the axial quadrupole moment  $\hat{Q}_{20}$ ), the quantities  $E(\mathbf{q}; T)$  and  $S(\mathbf{q}; T)$  are used to reconstruct the relation  $E(\mathbf{q}; S)$  by regression. For each temperature  $T$ , the curves  $E(\mathbf{q}; S)$  are then generated by fixing the entropy at its value at the top of the second barrier for that temperature  $T$ . Note that we could choose the entropy at other deformations: when properly normalized, the Maxwell relations guarantee that all these choices should be strictly equivalent, within the numerical accuracy of the regression. Figure 2 indicates that this accuracy is of the order of 500 keV at worst. This confirms earlier calculations [25, 60].

The isentropic representation of the fission process is often thought of as more physically justified than the isothermal one, as it has its origin in the separation of scales between the slow collective motion and fast intrinsic excitations of the nucleus [44, 61]. This separation justifies the thermodynamical assumption of adiabaticity [62]: going from point  $\mathbf{q}$  to point  $\mathbf{q}'$  in the collective space can be accomplished via a quasi-static, reversible transformation that conserves entropy. By contrast, it is sometimes argued that the absence of a heat bath to maintain the temperature constant invalidates the isothermal representation [20].

Such a statement, however, comes from a misconception about the nature of the heat bath. Indeed, another way to interpret the separation of scales between collective and intrinsic motion is to write the energy density of the fissioning nucleus as

$$\mathcal{H} = \mathcal{H}_{\text{coll}}(\mathbf{q}) + \mathcal{H}_{\text{int}}, \quad (14)$$

with the collective part depending only on the collective coordinates  $\mathbf{q}$  while the intrinsic part depends on all intrinsic degrees of freedom. In a DFT picture, for example, we would take  $\mathcal{H}_{\text{int}} = \mathcal{H}_{\text{int}}[\rho, \kappa]$ . The number of intrinsic degrees of freedom is given by the value of  $\rho$  and  $\kappa$  at every point in space, spin and isospin space: it is considerably higher than the number of collective variables. In addition, in the limit of no dissipation, the couplings between the two types of motion can be neglected [44]. The decomposition (14), together with the different relaxation scales, shows that the role of the heat bath is in fact played by the intrinsic Hamiltonian. In the theory of quantum dissipation, the latter is often modeled by a collection of harmonic oscillators [63, 64]. Passing from point  $\mathbf{q}$  to point  $\mathbf{q}'$  can thus also be accomplished through an isothermal process, during which heat will be exchanged between the collective wave-packet and the



intrinsic excitations, according to  $\delta Q = TdS$ . In our opinion, the two representations, which are mathematically equivalent thanks to the Maxwell equations, are also physically equivalent since they only rely on the hypothesis of the separation of degrees of freedom into slow collective and fast intrinsic motion.

To conclude this section, we note that, in order for the Maxwell relations to be valid, the respective thermodynamical potentials  $F(\mathbf{q})|_T$  and  $E(\mathbf{q})|_S$  must be differentiable at point  $\mathbf{q}$ . As discussed in Sec. IV E, this may not be true near scission, at least in the 4-d collective space explored in Fig. 2.

### B. Dependence of Fission Barriers on Excitation Energy

Fission barrier heights (both inner and outer barriers) are particularly important quantities in fission models, as they are often used as input to reaction codes. In Fig. 3, we show the variation of the inner and outer fission barrier heights in  $^{240}\text{Pu}$  as a function of the incident neutron energy  $E_n$ . As outlined in Sec. II A, we compute the fission barrier at incident neutron energy  $E_n$  for the entropy  $S$  such that  $E_n = U(S)$ . The maximum allowable thermal excitation energy is deduced from the  $E(\mathbf{q})|_S$  curves, which are obtained by spline interpolation over the  $F(\mathbf{q})|_T$  calculations. Note that at any point  $\mathbf{q}$ , the error on the total energy at given entropy due to the interpolation is smaller than 50 keV.

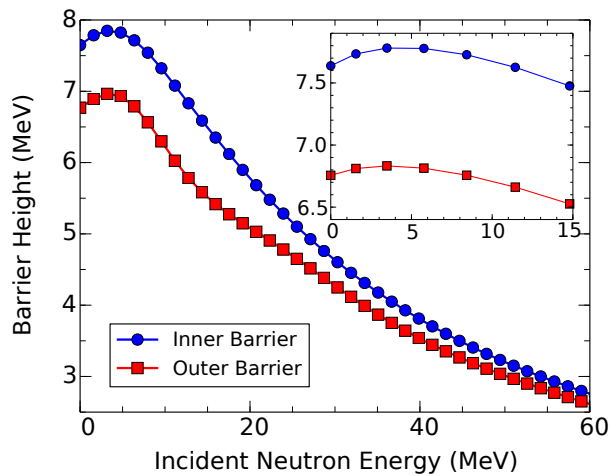


FIG. 3. (color online) Evolution of the inner and outer barrier heights in  $^{240}\text{Pu}$  as a function of the energy of the incident neutron. The inset represents a close-up in the 0 – 15 MeV region.

In the literature, fission barriers at finite temperature were computed within the macroscopic-microscopic approach [65–68], the semi-classical Thomas-Fermi framework [15–20], and the self-consistent HF theory [19, 21]. There are also a few applications of the finite-

temperature HFB theory with both zero-range Skyrme functionals and finite-range Gogny forces [24, 25, 69]. All these studies point to the disappearance of the barriers with the excitation energy of the compound nucleus, or equivalently, the nuclear temperature. Our results confirm this overall trend.

However, we emphasize here that this phenomenon occurs at temperatures that are relatively high as far as applications of neutron-induced fission are concerned. In the regime  $0 \leq E_n < 5 - 6$  MeV, the somewhat unexpected effect of nuclear temperature is to slightly *increase* fission barriers. In the inset of figure 3, we show a close-up of the fission barrier heights in the region  $0 \leq E_n < 15$  MeV. There is a very clear upward trend at low neutron energies. Although the increase of the fission barriers does not exceed 200 keV, the effect may be significant enough to affect fission fragment distributions.

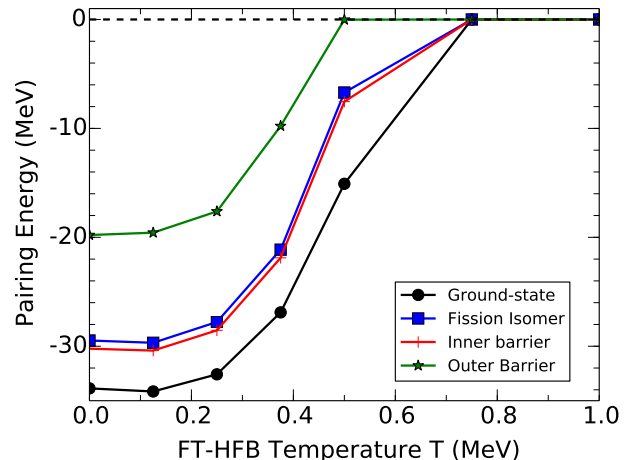


FIG. 4. (color online) Evolution of pairing energy in the ground-state, fission isomer, at the top of the first barrier and at the top of the second barrier in  $^{240}\text{Pu}$  as a function of the FT-HFB nuclear temperature.

The reason for the counter-intuitive behavior of the barriers may be attributed to the different damping speeds of pairing correlations and shell effects with temperature. In figure 4, we show the pairing energy as a function of the FT-HFB temperature for the ground-state, fission isomer, top of the first barrier and top of the second barrier in  $^{240}\text{Pu}$ . We find that pairing correlations have vanished completely beyond  $T = 0.75$  MeV, which corresponds to a neutron energy of approximately 12 MeV. However, shell effects are still substantial at this temperature [22]. Our interpretation is that the fast damping of pairing correlations attenuates, delays, or even partially reverts the impact of the damping of shell effects on the deformation energy as a function of temperature. Indeed, one of the side-effects of pairing correlations is to reduce deformation energy [40, 70], i.e., the energy difference  $E_{\text{def}}(\mathbf{q}) = E(\mathbf{q}) - E(\mathbf{q} = 0)$ . If pairing correlations rapidly decrease as a function of  $T$ , the

absolute value of the deformation energy may slightly increase as a result. Of course, this qualitative interpretation should be validated by rigorous macroscopic-microscopic calculations.

#### IV. FISSION FRAGMENT PROPERTIES AT FINITE TEMPERATURE

In (I), we discussed the fission fragment properties of  $^{239}\text{Pu}(n,f)$  at  $T = 0$  using the Joint Contour Net (JCN) to define a scission region in terms of topological changes of the density – based on the assumption that the variations of the density in the pre-fragments must be commensurate with those of the density in the compound nucleus. Within this region of scission configurations, we then apply a quantum localization method to disentangle the pre-fragments in order to approach the asymptotic conditions of two fully independent fragments. In this section, we extend this study to finite temperature.

##### A. Definition of a Scission Region

The fission pathway of lowest free energy across the 4-dimensional collective space shown in Fig. 2 was extended up to the scission region for each temperature. We find that the value  $q_{20}^{(\text{disc})}$  of the axial quadrupole moment where the first discontinuity in the  $F(q_{20})$  curve appears changes with temperature. Table I lists these values as a function of the temperature for the SkM\* functional. Note that there is a numerical uncertainty of about 2–3 b for the values of  $q_{20}$  reported in the table, since calculations converge very slowly near scission. The scission region covers a relatively broad range of  $\hat{Q}_{20}$  values of approximately 25 b. Note the original increase of the quadrupole moment at low temperatures: this is caused by the quenching of pairing correlations, which was shown to shift the discontinuity at larger values of  $\hat{Q}_{20}$  in (I). Since the discontinuity does not occur at the same  $q_{20}$  for all temperatures, the equivalence between the  $E(q_{20})|_S$  and  $F(q_{20})|_T$  representations of the fission pathway does not hold in the scission region since neither the internal energy nor the free energy are continuous functions over the entire range of quadrupole moments involved.

TABLE I. Position of the first discontinuity of the  $F(q_{20})$  curve along the most probably fission pathway as a function of temperature.

T (MeV)	$q_{20}^{(\text{disc})}$ (b)	T (MeV)	$q_{20}^{(\text{disc})}$ (b)
0.00	345.0	1.00	332.5
0.25	357.0	1.25	331.0
0.50	339.5	1.50	333.0
0.75	332.0	1.75	333.0

Following the approach at zero-temperature outlined in (I), we introduce an additional constraint on the number of particles in the neck,  $\hat{Q}_N$ , to explore scission configurations. At each temperature  $T$ , the expectation value of  $\hat{Q}_N$  is varied in the range  $q_N \in [0.1, 4.5]$ , while the quadrupole moment is fixed at the values listed in Table I. The JCN analysis is then applied at each temperature to the set of neutron and proton densities along these trajectories to identify putative scission configurations. As illustration, figure 5 shows the JCN at  $q_N = 0.2$  at both  $T = 0.0$  MeV (top) and  $T = 1.5$  MeV (bottom).

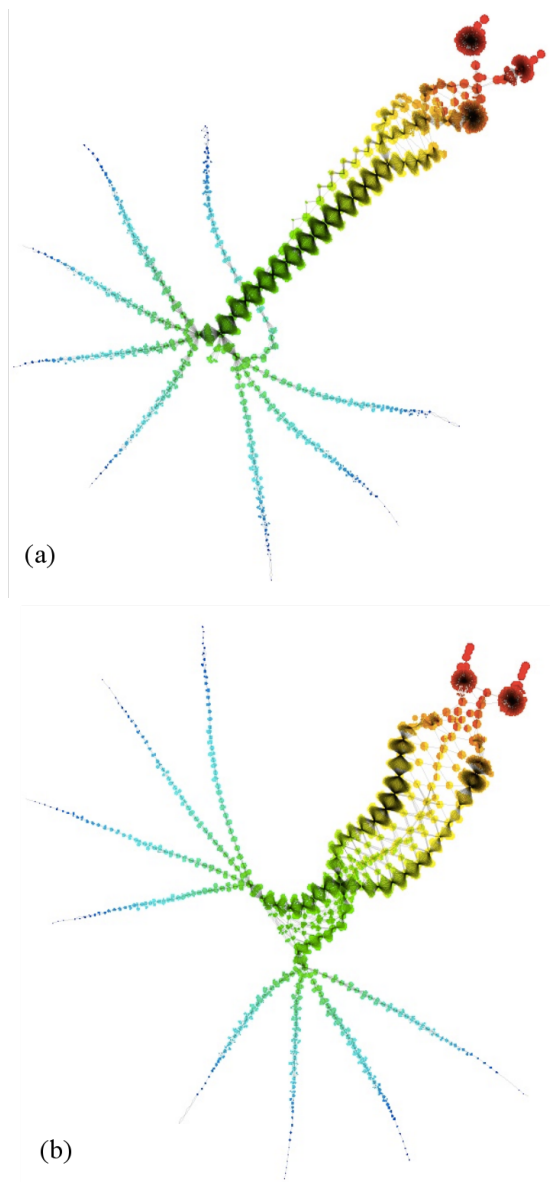


FIG. 5. (color online) Joint Contour Net graph of the densities at  $q_N = 0.2$  at temperature  $T = 0.00$  MeV (a) and  $T = 1.50$  MeV (b).

We recall that the JCN algorithm provides a computational tool for extracting the topological features of a multifield dataset, which includes connectivity between



regions of different behaviors. It was first introduced in the context of nuclear structure in Ref. [71] and applied in (I) to the specific problem of defining scission configurations along a continuous fission pathway for neutron-induced fission. The JCN analysis involves generalizing one-dimensional scalar analysis to capture simultaneous variation in multiple output functions of the type  $(f_1, \dots, f_n) : \mathbb{R}^3 \rightarrow \mathbb{R}^n$ . In (I), we concluded that the JCN could be a useful tool to define plausible scission configurations. In particular, the appearance of a branching structure in the JCN, which characterizes the existence of two distinct regions in space, was interpreted as the precursor to scission; the subsequent development of “starbursts” in each branch was associated with the completion of scission, as these startbursts indicate that the variations of the density in each fragment is commensurate to those of the density in the whole nucleus (hence, suggesting two well-defined fragments). We also observed that this identification is independent of the numerical parameters used in the JCN.

TABLE II. Interval  $I_q = [q^{(\min)}, q^{(\max)}]$  of scission configurations as obtained from the JCN analysis of  $^{240}\text{Pu}$  as a function of the temperature  $T$ .

T (MeV)	$q^{(\min)}$	$q^{(\max)}$	T (MeV)	$q^{(\min)}$	$q^{(\max)}$
0.00	0.2	2.6	1.00	0.3	3.1
0.25	0.2	2.5	1.25	0.5	3.1
0.50	0.2	2.8	1.50	0.5	3.1
0.75	0.2	3.0	1.75	0.7	3.1

The results of the JCN analysis for the least energy fission pathway of  $^{240}\text{Pu}$  at finite temperature are summarized in Table II. As in (I), we define an interval  $I_q = [q^{(\min)}, q^{(\max)}]$  in the collective space, with  $q^{(\min)}$  the value of  $\hat{Q}_N$  where scission has completed (=the actual scission point), and  $q^{(\max)}$  the value corresponding to the precursor to scission. We note that the precursor value is relatively stable, especially at high temperatures, while the position of the scission point, which is constant up to  $T = 1.0$  MeV, moves to thicker necks beyond  $T > 0.75$  MeV. We will return to this result in Sec. IVE.

The JCN also picked up an interesting “zippering effect” of the datasets (the proton and neutron densities) at large temperatures and low  $q_N$  values. This effect is illustrated in Fig. 5, which shows the JCN at  $q_N = 0.2$  at both  $T = 0.0$  MeV (top) and  $T = 1.5$  MeV (bottom). In both cases, the fragments are clearly formed as evidenced by the two distinct branches in the upper right side of each figure. In addition, we notice at  $T = 1.5$  MeV a complex pattern connecting the two fragments, which look similar to a zipper. We have found that this pattern becomes more noticeable for  $T \geq 1.25$  MeV. Since the zippering connects the two pre-fragments, it should be indicative of a spatial connection between these two distinct regions of space; in addition, the effect manifests itself only at temperatures where the coupling to the continuum be-

comes sizable, see Sec. IV D. Therefore, we suggest that the zippering effect of the JCN is the representation of a spatial delocalization of quasiparticles (mostly neutrons) at large temperatures.

## B. Quasi-Particle Occupations

The generalization at  $T > 0$  of the procedure to identify a left and a right fragment, their observables and their interaction energy presented in (I) is straightforward. Using the definition (9) for the one-body density matrix at finite temperature  $T > 0$ , we find that the coordinate space representation  $\rho_\mu(\mathbf{r}\sigma, \mathbf{r}'\sigma')$  of the density of a single quasi-particle  $\mu$  reads

$$\rho_\mu(\mathbf{r}\sigma, \mathbf{r}'\sigma') = \sum_{ij} [V_{i\mu}^*(1 - f_\mu)V_{j\mu} + U_{i\mu}f_\mu U_{j\mu}^*] \times \phi_i(\mathbf{r}\sigma)\phi_j^*(\mathbf{r}'\sigma'), \quad (15)$$

with  $\phi_i(\mathbf{r}\sigma)$  the single-particle basis functions. With this definition, the spatial occupation  $N_\mu$  of the q.p.  $\mu$  and the total number of particles  $N$  are formally the same as at  $T = 0$ , that is,

$$N_\mu = \sum_{\sigma} \int d^3\mathbf{r} \rho_\mu(\mathbf{r}\sigma, \mathbf{r}\sigma), \quad (16)$$

and

$$N_\mu = \sum_i [V_{i\mu}^*(1 - f_\mu)V_{i\mu} + U_{i\mu}f_\mu U_{i\mu}^*]. \quad (17)$$

As in (I), we introduce the quantity

$$d_{ij}(z) = \sum_{\sigma} \int_{-\infty}^{+\infty} dx \int_{-\infty}^{+\infty} dy \int_{-\infty}^z dz \phi_i(\mathbf{r}\sigma)\phi_j^*(\mathbf{r}\sigma). \quad (18)$$

Still assuming that the neck between the two fragments is located on the  $z$ -axis of the intrinsic reference frame, and thus has the coordinates  $\mathbf{r}_{\text{neck}} = (0, 0, z_N)$ , we can define the occupation of the q.p. in the fragment (1) as

$$N_{1,\mu} = \sum_{ij} [V_{i\mu}^*(1 - f_\mu)V_{j\mu} + U_{i\mu}f_\mu U_{j\mu}^*] d_{ij}(z_N), \quad (19)$$

As at  $T = 0$ , the occupation of the q.p. in the fragment (2) is simply  $N_{2,\mu} = N_\mu - N_{1,\mu}$ . We then assign the q.p.  $\mu$  to fragment (1) if  $N_{1,\mu} \geq 0.5N_\mu$ , and to fragment (2) if  $N_{1,\mu} < 0.5N_\mu$ . This gives us two sets of quasiparticles. For each of them, we can define the corresponding pseudodensities and pseudo pairing tensor. For fragment (f) we find, in coordinate $\otimes$ spin space,

$$\rho^{(f)}(\mathbf{r}\sigma, \mathbf{r}'\sigma') = \sum_{\mu \in (f)} \sum_{ij} [V_{i\mu}^*(1 - f_\mu)V_{j\mu} + U_{i\mu}f_\mu U_{j\mu}^*] \phi_i(\mathbf{r}\sigma)\phi_j^*(\mathbf{r}'\sigma'), \quad (20)$$

$$\kappa^{(f)}(\mathbf{r}\sigma, \mathbf{r}'\sigma') = \sum_{\mu \in (f)} \sum_{ij} [V_{i\mu}^*(1 - f_\mu)U_{j\mu} + U_{i\mu}f_\mu V_{j\mu}^*] \phi_i(\mathbf{r}\sigma)\phi_j^*(\mathbf{r}'\sigma'). \quad (21)$$

These are the equivalent at  $T > 0$  of Eqs.(12)-(13) in (I). We can build the analog of the kinetic energy density and the spin current tensor from these pseudodensities. The Coulomb and nuclear interaction energy between the two fragments thus takes the same form as at  $T = 0$ , only the definition of the various pseudodensities is modified according to Eq.(9) and Eq.(20).

### C. Quantum Localization at Finite Temperature

As recalled in (I), at  $T = 0$  the localization method of Ref. [72] is based on the idea that any unitary transformation of the q.p. operators  $(\beta^\dagger, \beta)$  leaves the generalized density matrix, hence all global observables such as the total energy, radii, etc., invariant. In this section, we generalize this result at  $T > 0$  and discuss how it impacts the practical implementation of the method.

#### 1. Unitary Transformation of Quasiparticles

As in (I), we consider the following unitary transformation  $\hat{T}$  of the eigenvectors of the HFB matrix,

$$A_\alpha \equiv \hat{T}U_\mu = \sum_\mu T_{\alpha\mu}U_\mu, \quad (22)$$

$$B_\alpha \equiv \hat{T}V_\mu = \sum_\mu T_{\alpha\mu}V_\mu \quad (23)$$

where the quantities  $A_\alpha$ ,  $B_\alpha$ ,  $U_\mu$  and  $V_\mu$  are in fact vectors with  $N$  components  $A_{n\alpha}$  in the original s.p. basis, so that, in matrix form,

$$A = UT^T, \quad B = VT^T. \quad (24)$$

It is straightforward to notice that the matrix  $\mathcal{W}'$  defined as

$$\mathcal{W}' = \begin{pmatrix} A & B^* \\ B & A^* \end{pmatrix} = \begin{pmatrix} U & V^* \\ V & U^* \end{pmatrix} \mathcal{T}^\dagger = \mathcal{W}\mathcal{T}^\dagger, \quad (25)$$

with

$$\mathcal{T} = \begin{pmatrix} T^* & 0 \\ 0 & T \end{pmatrix}, \quad \mathcal{T}\mathcal{T}^\dagger = \mathcal{T}^\dagger\mathcal{T} = 1, \quad (26)$$

verifies  $\mathcal{W}'\mathcal{W}'^\dagger = \mathcal{W}'^\dagger\mathcal{W}' = 1$ . The matrices  $A$  and  $B$  thus define new sets of q.p. operators  $(\eta^\dagger, \eta)$  such that

$$\eta_\alpha = \sum_\mu T_{\alpha\mu}^*\beta_\mu, \quad \eta_\alpha^\dagger = \sum_\mu T_{\alpha\mu}\beta_\mu^\dagger. \quad (27)$$

Therefore, a unitary transformation of the Bogoliubov matrices of the type (22)-(23) correspond to a transformation of the q.p. creation (annihilation) operators into linear combination of themselves without mixing creation and annihilation operators [13].

Using the Baker-Hausdorff Campbell formula, it is not very difficult to show that, for the form (27) of the unitary transformation there exists in Fock space a general transformation rule for the q.p. operators

$$\eta_\mu = e^{i\hat{R}}\beta_\mu e^{-i\hat{R}}, \quad \eta_\mu^\dagger = e^{i\hat{R}}\beta_\mu^\dagger e^{-i\hat{R}}, \quad (28)$$

where  $\hat{R}$  is a one-body Hermitian operator written in the original q.p. basis as  $\hat{R} = \sum_{\mu\nu} R_{\mu\nu}\beta_\mu^\dagger\beta_\nu$ .

#### 2. General Invariance of the Density Matrix at $T > 0$

We now prove that the one-body density matrix  $\rho_{ij}$  of Eq.(9) is invariant under a rotation of the q.p. operators. More precisely: if we start from a HFB vacuum corresponding to the rotated q.p. operators  $\eta$  and compute the one-body density matrix by using the Bogoliubov transformation  $\mathcal{W}'$ , the result is the same as if we had started from the HFB vacuum of the  $\beta$  operators using the initial Bogoliubov transformation  $\mathcal{W}$ .

The statistical trace defining  $\rho_{ij}$  can be computed in any arbitrary many-body basis  $|n\rangle$  of the Fock space. Generically, we thus have

$$\rho_{ij} = \sum_n \langle n | \hat{D} c_j^\dagger c_i | n \rangle. \quad (29)$$

Let us introduce the new set of q.p. operators  $\eta$  obtained by the unitary transformation of Eq.(27). We choose the multi-qp states  $|n\rangle$  of Eq.(29) from the vacuum of the rotated q.p. operators, that is,

$$|n\rangle \equiv |\eta_n\rangle = \eta_1^\dagger \cdots \eta_n^\dagger |\text{vac}_\eta\rangle. \quad (30)$$

Then, we introduce the Bogoliubov transformation  $\mathcal{W}'$  to express the  $c$  operators as a function of the  $\eta$  operators. We find

$$\rho_{ij} = \sum_{\mu\nu} B_{j\mu} B_{i\nu}^* \sum_n \langle \eta_n | \hat{D} \eta_\mu \eta_\nu^\dagger | \eta_n \rangle + \sum_{\mu\nu} A_{j\mu}^* A_{i\nu} \sum_n \langle \eta_n | \hat{D} \eta_\mu^\dagger \eta_\nu | \eta_n \rangle, \quad (31)$$

We now use the property (28) to express the multi-qp states  $|\eta_n\rangle$  of the  $\eta$  operators as a function of the multi-qp states  $|\beta_n\rangle$  of the  $\beta$  operators. By definition of the multi-qp states, we find

$$|\eta_n\rangle = \eta_1^\dagger \cdots \eta_n^\dagger |\text{vac}_\eta\rangle = e^{i\hat{R}} |\beta_n\rangle. \quad (32)$$

Above, we have used the property  $e^{-i\hat{R}} |\text{vac}_\eta\rangle = |\text{vac}_\beta\rangle$ . This property is the direct consequence of the definition of the vacuum: it is the state such that, for all vectors  $v$  of the Fock space and any index  $i$ ,  $\langle v | \eta_i | \text{vac}_\eta \rangle = 0$ . Defining  $|w\rangle = e^{-i\hat{R}} |v\rangle$ , we find  $\langle w | \beta_i e^{-i\hat{R}} | \text{vac}_\eta \rangle = 0$ . Hence,  $e^{-i\hat{R}} |\text{vac}_\eta\rangle$  is the vacuum for operators  $\beta_i$ , since the property is valid for all  $|w\rangle$ . Since the vacuum is



As a consequence of the non-diagonal form of  $\tilde{\mathcal{R}}'$ , the one-body density matrix cannot be expressed as a simple sum over single quasiparticle densities. This implies that the coordinate space representation of  $\rho$  becomes

$$\rho(\mathbf{r}\sigma, \mathbf{r}'\sigma') = \sum_{k \in \mathcal{S}} \rho_k(\mathbf{r}\sigma, \mathbf{r}'\sigma') + \sum_{\mu\nu \in \mathcal{P}} \rho'_{\mu\nu}(\mathbf{r}\sigma, \mathbf{r}'\sigma'), \quad (49)$$

where  $\mathcal{S}$  refers to the set of q.p. that are not rotated, and  $\mathcal{P}$  to the set of q.p. that are rotated. The contribution  $\rho'_{\mu\nu}(\mathbf{r}\sigma, \mathbf{r}'\sigma')$  of the rotated pair  $(\mu, \nu)$  of quasiparticles to the total one-body density (which is invariant) is

$$\begin{aligned} \rho'_{\mu\nu}(\mathbf{r}\sigma, \mathbf{r}'\sigma') &= \sum_{ij} \phi_i(\mathbf{r}\sigma) \phi_j^*(\mathbf{r}'\sigma') \times \\ &[B_{i\mu}^* G'_{\mu\mu} B_{j\mu} + A_{i\mu} F'_{\mu\mu} A_{j\mu}^* + B_{i\mu}^* G'_{\mu\nu} B_{j\nu} + A_{i\mu} F'_{\mu\nu} A_{j\nu}^* \\ &+ B_{i\nu}^* G'_{\nu\mu} B_{j\mu} + A_{i\nu} F'_{\nu\mu} A_{j\mu}^* + B_{i\nu}^* G'_{\nu\nu} B_{j\nu} + A_{i\nu} F'_{\nu\nu} A_{j\nu}^*]. \end{aligned} \quad (50)$$

For rotated q.p., the notion of spatial occupation cannot be captured by the quantity  $N_\mu$  alone. We thus redefine the spatial occupation of the rotated pairs  $(\mu, \nu)$  and  $(\nu, \mu)$  of quasiparticles by

$$\begin{aligned} N'_{\mu\nu} &= \sum_i [B_{i\mu}^* G'_{\mu\mu} B_{i\mu} + A_{i\mu} F'_{\mu\mu} A_{i\mu}^*] \\ &+ \sum_i [B_{i\mu}^* G'_{\mu\nu} B_{i\nu} + A_{i\mu} F'_{\mu\nu} A_{i\nu}^*] \end{aligned} \quad (51)$$

and

$$\begin{aligned} N'_{\nu\mu} &= \sum_i [B_{i\nu}^* G'_{\nu\nu} B_{i\nu} + A_{i\nu} F'_{\nu\nu} A_{i\nu}^*] \\ &+ \sum_i [B_{i\nu}^* G'_{\nu\mu} B_{i\mu} + A_{i\nu} F'_{\nu\mu} A_{i\mu}^*] \end{aligned} \quad (52)$$

Note that  $N'_{\mu\nu} \neq N'_{\nu\mu}$ . A tedious but straightforward calculation shows that  $N'_{\mu\nu} + N'_{\nu\mu} = N_\mu + N_\nu$ , which is nothing but the consequence of the invariance of the density matrix under this rotation. Similarly, the spatial occupations in the fragment (1) of the rotated pair  $(\mu, \nu)$  and  $(\nu, \mu)$  of quasiparticles now read

$$\begin{aligned} N'_{1,\mu\nu} &= \sum_{ij} [B_{i\mu}^* G'_{\mu\mu} B_{j\mu} + A_{i\mu} F'_{\mu\mu} A_{j\mu}^*] d_{ij}(z_N) \\ &+ \sum_{ij} [B_{i\mu}^* G'_{\mu\nu} B_{j\nu} + A_{i\mu} F'_{\mu\nu} A_{j\nu}^*] d_{ij}(z_N) \end{aligned} \quad (53)$$

and

$$\begin{aligned} N'_{1,\nu\mu} &= \sum_{ij} [B_{i\nu}^* G'_{\nu\nu} B_{j\nu} + A_{i\nu} F'_{\nu\nu} A_{j\nu}^*] d_{ij}(z_N) \\ &+ \sum_{ij} [B_{i\nu}^* G'_{\nu\mu} B_{j\mu} + A_{i\nu} F'_{\nu\mu} A_{j\mu}^*] d_{ij}(z_N) \end{aligned} \quad (54)$$

This simple extension reflects the fact that the two quasiparticles forming the pair are not independent anymore.

#### 4. Implementation of the Quantum Localization at $T > 0$

In practice, we construct the fission fragments by scanning both the set  $\mathcal{S}$  of non-rotated q.p. and the set  $\mathcal{P}$  of rotated q.p.:

- For all q.p.  $\mu \in \mathcal{S}$ , we compute  $N_\mu$ ,  $N_{1,\mu}$  and  $N_{2,\mu}$  according to Eq.(17) and Eq.(19); the q.p. is assigned to fragment (1) if  $N_{1,\mu} \geq 0.5N_\mu$ , to fragment (2) otherwise;
- Let us note  $\mathcal{P}_\mu = (\mu, \nu)$  the pair of q.p.  $\mu$  and  $\nu$ . We have  $\mathcal{P} = \bigcup \mathcal{P}_\mu$ . For each pair  $\mathcal{P}_\mu$ , and for each q.p.  $\mu$  in this pair, we compute  $N'_{\mu\nu}$ ,  $N'_{1,\mu\nu}$  and  $N'_{2,\mu\nu}$  according to Eqs.(51)-(54); the q.p.  $\mu$  is assigned to fragment (1) if  $N'_{1,\mu\nu} \geq 0.5N'_{\mu\nu}$ , to fragment (2) otherwise. Note that the procedure must be done separately for the q.p.  $\mu$  of and the q.p.  $\nu$  of the pair, since  $N'_{\mu\nu} \neq N'_{\nu\mu}$ .

The result of this procedure is to partition the whole set of quasiparticles into two subsets corresponding to the two fragments. The pseudodensities in the fragment can then be formally written as

$$\begin{aligned} \rho'^{(f)}(\mathbf{r}\sigma, \mathbf{r}'\sigma') &= \sum_{\mu \in (f)} \sum_{\nu \in \mathcal{P}_\mu} \sum_{ij} [B_{i\mu}^* G'_{\mu\nu} B_{j\nu} \\ &+ A_{i\mu} F'_{\mu\nu} A_{j\mu}^*] \phi_i(\mathbf{r}\sigma) \phi_j^*(\mathbf{r}'\sigma'), \end{aligned} \quad (55)$$

$$\begin{aligned} \kappa'^{(f)}(\mathbf{r}\sigma, \mathbf{r}'\sigma') &= \sum_{\mu \in (f)} \sum_{\nu \in \mathcal{P}_\mu} \sum_{ij} [B_{i\mu}^* G'_{\mu\nu} A_{j\nu} \\ &+ A_{i\mu} F'_{\mu\nu} B_{j\nu}^*] \phi_i(\mathbf{r}\sigma) \phi_j^*(\mathbf{r}'\sigma'). \end{aligned} \quad (56)$$

These relations allow to extend the calculation of the interaction energy between the fragments and the fragment internal energies at  $T > 0$  using the formulas given in (I).

We have implemented the localization method in a new module of the DFT solver HFODD [57]. The rotation of the q.p. is first performed in the s.p. space, i.e., the matrices  $U$  and  $V$  of the Bogoliubov transformation are rotated according to Eq.(25). Using Eq.(9) and Eq.(33), we have checked that the density matrix in the s.p. basis (the deformed HO basis in our case) remains invariant after the transformation within numerical precision.

In HFODD, calculations of the nuclear and Coulomb interaction energy are carried out in coordinate space. The matrices of the Bogoliubov transformation are first transformed into spinors according to

$$\begin{aligned} \varphi_\mu^{(1)}(\mathbf{r}\sigma) &= -2\sigma \sum_i U_{i\mu}^* \phi_i^*(\mathbf{r} - \sigma), \\ \varphi_\mu^{(2)}(\mathbf{r}\sigma) &= \sum_i V_{i\mu}^* \phi_i(\mathbf{r}\sigma), \end{aligned} \quad (57)$$

Note that this transformation depends on a specific phase convention. Local densities are then defined in terms of these HFB spinors; see [73] for details. We have then checked that the coordinate space representations of the densities, as computed from the HFB spinors (57) are

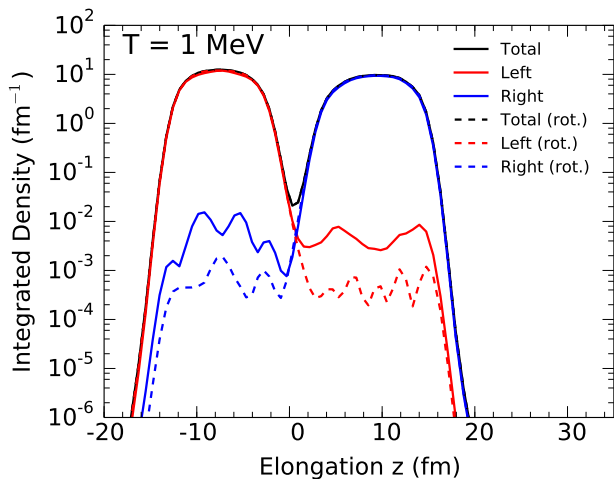


FIG. 6. (color online) Profile of the integrated nuclear density  $\rho(\mathbf{z})$  (integrated over  $x$ - and  $y$ - coordinates) along the elongation axis  $z$  in  $^{240}\text{Pu}$  at  $q_N = 0.7$  and  $T = 1.0$  MeV before (plain lines) and after (dashed lines) rotation of the q.p. wave-functions.

also invariant after the q.p. rotation within machine precision.

As an example, figure 6 shows the impact of the localization on the pseudodensities of the fission fragments. The figure shows the one-body density matrix of the compound nucleus before and after rotation; it also shows the pseudodensities of the left and right fragment, before and after rotation. All densities were integrated along the  $x$ - and  $y$ -directions. As at  $T = 0$ , we observe a significant decrease of the tails of the densities, of approximately an order of magnitude. The curves labeled “Total” and “Total (rot.)”, which pertain to the total density before and after rotation, are indistinguishable.

#### D. Coupling to the Continuum

It was demonstrated in Refs. [49, 50] based on the coordinate space formulation of the HFB equations (in spherical symmetry) that the asymptotic conditions for the  $(U, V)$  matrices of the Bogoliubov transformations read

$$U(E, r\sigma) \rightarrow \begin{cases} \cos(k_1 r + \delta_1) & E > -\lambda \\ e^{-\kappa_1 r} & E < -\lambda \end{cases} \quad (58)$$

$$V(E, r\sigma) \rightarrow \begin{cases} \cos(k_1 r + \delta_1) & E < +\lambda \\ e^{-\kappa_1 r} & E > +\lambda \end{cases} \quad (59)$$

From these expressions, it was shown that for nuclei with negative Fermi energy, the local density is always localized, which leads to observables taking finite values.

At  $T > 0$ , the FT-HFB equations take exactly the same form as at  $T = 0$ , hence the matrices  $U$  and  $V$  of the Bogoliubov transformation have the same asymptotic properties. We summarize in Table III the localized or

delocalized nature of the  $U$  and  $V$  matrices of the Bogoliubov transformation depending on the value of the Fermi level  $\lambda$  and the energy  $E$  of the q.p..

TABLE III. Localization properties at  $T > 0$  of the matrices  $(U, V)$  of the Bogoliubov transformation depending on the value of the q.p. energies and the Fermi level.

Fermi Level	q.p. Energy	Localization of $(U, V)$
$\lambda > 0$	$E > +\lambda$	$U$ delocalized, $V$ localized
	$E < +\lambda$	$U$ delocalized, $V$ delocalized
$\lambda < 0$	$E > -\lambda$	$U$ delocalized, $V$ localized
	$E < -\lambda$	$U$ localized, $V$ localized

Contrary to the case at  $T = 0$ , however, the density matrix now takes the form of Eq.(9), and the additional term  $fUU^\dagger$  can be delocalized even for systems with negative Fermi energy. In fact, the set of quasi-particles can be split into the subset  $\mathcal{L}$  of localized, discrete q.p, with  $0 \leq E < -\lambda$ , and the subset  $\mathcal{C}$  of delocalized, continuous q.p. with  $E > -\lambda$ . The full density is, of course, the sum of the two contributions

$$\rho_{ij} = \rho_{ij}^{(\text{loc})} + \rho_{ij}^{(\text{con})}, \quad (60)$$

with

$$\rho_{ij}^{(\text{loc})} = \sum_{\mu \in \mathcal{L}} (V_{i\mu}^* (1-f)_\mu V_{j\mu} + U_{i\mu} f_\mu U_{j\mu}^*), \quad (61)$$

and (assuming the continuous spectrum is discretized as, e.g. happens in the HO basis),

$$\rho_{ij}^{(\text{con})} = \sum_{\mu \in \mathcal{C}} (V_{i\mu}^* (1-f)_\mu V_{j\mu} + U_{i\mu} f_\mu U_{j\mu}^*). \quad (62)$$

In Fig. 7, we illustrate this result by showing the profile of the total isoscalar density  $\rho_0(\mathbf{r})$  along the elongation axis of  $^{240}\text{Pu}$  in the scission region, at  $q_N = 1.0$ , together with the contribution of the term  $fUU^\dagger$  to its delocalized contribution  $\rho_{ij}^{(\text{con})}$ . Curves are shown at  $T = 1.0, 1.5, 2.0$  MeV. At  $T = 1.0$  MeV, the energy of the incident neutron is of the order of 25 MeV, while it is more than 70 MeV at  $T = 2.0$  MeV. Yet, even at such a high excitation energy and after integrating over the transverse coordinates  $x$  and  $y$ , the contribution of the term  $fUU^\dagger$  to the total density is at most of the order of  $10^{-4}$ . We note that the use of the one-center HO basis induces numerical limitations: the tails of the densities at the boundaries of the domain are not physical but a consequence of the Gaussian asymptotic behavior of the basis functions (which is visible as a roughly parabolic decrease of the density near  $z = \pm 20 - 25$  fm).

The densities can be further integrated over  $z$  to provide an estimate of the number of particles originating from the q.p. located in the continuum. This is shown in Fig. 8 as a function of  $q_N$  for five values of the nuclear temperature,  $T = 0, 0.5, \dots, 2.0$  MeV. For temperatures below 1.5 MeV, the number of particle is virtually

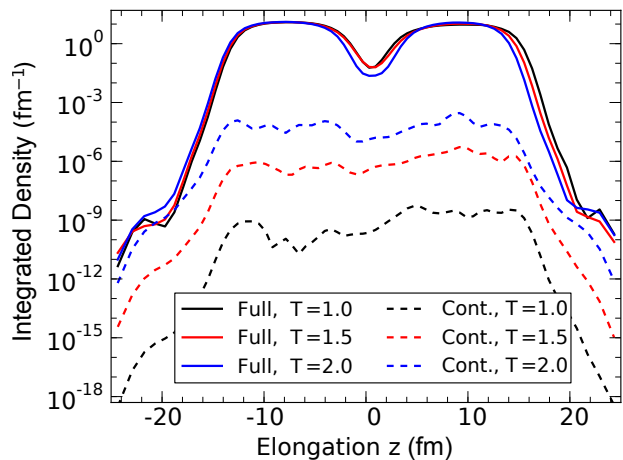


FIG. 7. (color online) Profile of the isoscalar nuclear density  $\rho_0(\mathbf{r})$  (integrated over  $x$ - and  $y$ - coordinates) along the elongation axis  $z$  in  $^{240}\text{Pu}$  at  $q_N = 1.0$  and  $T = 1.0, 1.5, 2.0$  MeV. The plain lines correspond to the full density, the dashed lines to the term  $fUU^\dagger$  only of  $\rho^{(\text{con})}$ .

zero; only beyond 1.5 MeV is the contribution noticeable, with up to about 1 particle in the continuum at  $T = 2.0$  MeV. Because of the unphysical spatial truncation of q.p. wave-functions induced by the asymptotic behavior of the basis functions, it may be possible that the actual coupling to the continuum is a little stronger. It is, however, unlikely that the effect is strong enough to have a sizable impact on the physics of neutron-induced fission.

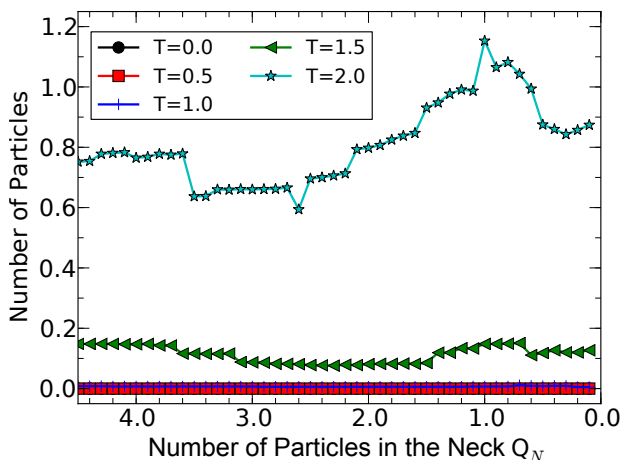


FIG. 8. (color online) Total number of delocalized quasi-particles as a function of the number of particles in the neck for various temperatures.

We have thus shown that, in the regime of temperatures relevant to the description of induced nuclear fission, the coupling to the continuum remains essentially negligible. Our results are fully compatible with esti-

mates published in the literature. Indeed, early works in the context of the finite-temperature Hartree-Fock theory suggested that the effect of the continuum becomes significant only at  $T > 4$  MeV [52]. In the follow-up paper by the same authors, the density of neutron vapor in  $^{208}\text{Pb}$  was shown to be  $0.510^{-2} \text{ fm}^{-3}$  at  $T = 7$  MeV [51]. More recent estimates obtained at the fully FT-HFB level with a coordinate-space solver also suggest a total number of particles in the continuum of 0.2 at  $T = 1.5$  MeV in the superheavy element  $Z = 114, N = 178$  [25]. These results are noteworthy, because they justify *a posteriori* the validity of the model of the compound nucleus to describe induced fission.

### E. Fragment Interaction Energy and Kinetic Energy

Based on the JCN analysis presented in Sec. IV A, we have identified the range  $q_N \in [0.1-3.0]$  as the scission region, with  $q_N \approx 0.2-0.3$  as the most likely scission point (at low temperatures). Using the generalized quantum localization procedure of Sec. IV C, we have computed the fission fragment interaction energy and total kinetic energy before and after localization for the range of temperatures  $0 \leq T \leq 1.75$  MeV. For  $T \geq 1.50$  MeV, the localization method begins to break down: on the one hand, the number of possible pairs meeting the criteria for rotation becomes very large and the procedure becomes very time-consuming; in addition, it does not always succeed in fully localizing the fragments. This may be an indirect effect of the coupling to the continuum discussed in the previous section.

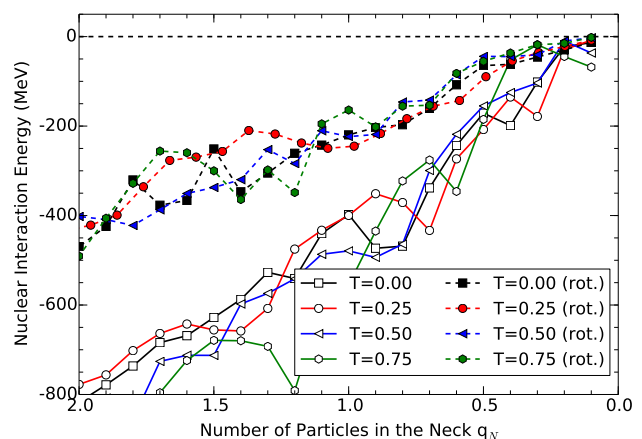


FIG. 9. (color online) Skyrme interaction energy between the fission fragments of  $^{240}\text{Pu}$  as a function of the number of particles in the neck for the SkM\* functional at low temperatures  $0.00 \leq T \leq 0.75$  MeV. Solid curves with open symbols correspond to the calculation before the localization is applied, dashed curves with filled symbols to the localized q.p.

It is interesting to distinguish two temperature



regimes. In the range  $0 \leq T \leq 0.75$  MeV, which is depicted in Fig. 9, there are relatively few qualitative differences between the zero-temperature case and the finite-temperature results: the nuclear interaction energy is of the same order of magnitude at all  $T$ , both before and after quantum localization. This is consistent with the earlier observation in Sec. III A that the potential energy surface does not change dramatically in this temperature range. As in (I), we note relatively large fluctuations of the interaction energy as a function of  $q_N$ , especially before localization. To a large extent, these fluctuations reflect the binary nature of the partitioning of the nucleus in two (entangled) fragments: a given q.p. could be assigned to one fragment for a given  $q_N$  and to the other at  $q_N + \delta q_N$ , especially if its localization  $\ell$  indicator is close to 0.5. After localization, such fluctuations are strongly attenuated but do not disappear entirely, since there remain a few q.p. that can not be properly localized [72]. In addition, small discontinuities in the unconstrained collective variables can also contribute to the fluctuations of interaction energy.

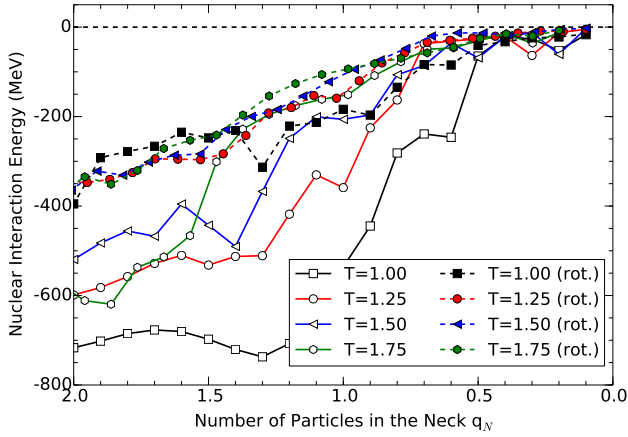


FIG. 10. (color online) Same as Fig. 9 in the higher temperature regimes  $1.00 \leq T \leq 1.75$  MeV.

In the higher temperature regime, the effect of changes in temperature becomes more visible. From a purely topological point of view, the scission point as determined by the JCN is pushed back from  $q_N \approx 0.2 - 0.4$  to  $q_N \approx 0.5 - 0.9$ . This observation is confirmed by the behavior of the nuclear interaction energy: As a function of  $q_N$ , the interaction energy goes to zero faster as  $T$  increases. This trend is already clearly visible before localization, the effect of which is to make it more pronounced. Qualitatively, these results show that the system tends to break with a thicker neck than at lower temperatures, in a manner somewhat similar to glass.

We show in Fig. 11 the variations of the direct Coulomb interaction energy along the  $q_N$  trajectory at low temperatures, which are the most relevant to applications of neutron-induced fission. We notice again the smoothing effect of the localization method, especially at large  $q_N$

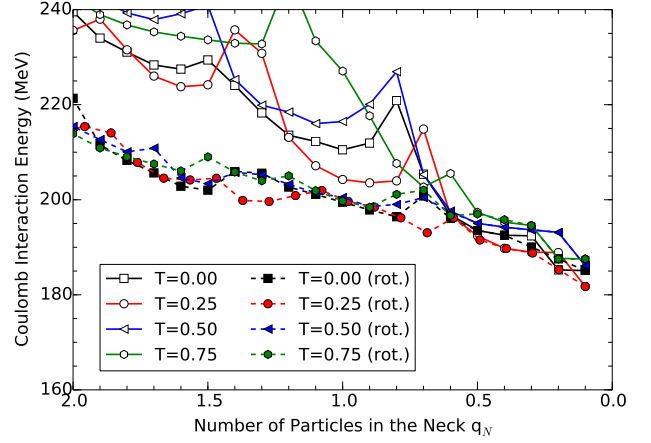


FIG. 11. (color online) Direct Coulomb interaction energy in the fission of  $^{240}\text{Pu}$  as a function of the number of particles in the neck for the SkM\* functional for temperatures in the range  $0.00 \leq T \leq 0.75$  MeV.

values, where the fragments are still heavily entangled. We also remark that the effect of the temperature is weak, which is compatible with experimental evidence, which a variation of about 2 MeV in TKE over a 5 MeV range of neutron energies [74]. For  $q_N = 0.2$ , which the JCN analysis identifies as the most likely scission configuration, the Coulomb interaction energy seems first to increase with temperature, from about 185 MeV up to approximately 195 MeV at  $T = 0.50$  MeV (corresponding to  $E^* \approx 8 - 10$  MeV excitation energy in the compound nucleus), before decreasing as temperature keeps on increasing. However, it is clear from the figure that the amplitude of the energy fluctuations along the  $Q_N$  path in the scission region are quite large, so these results should be taken with a grain of salt.

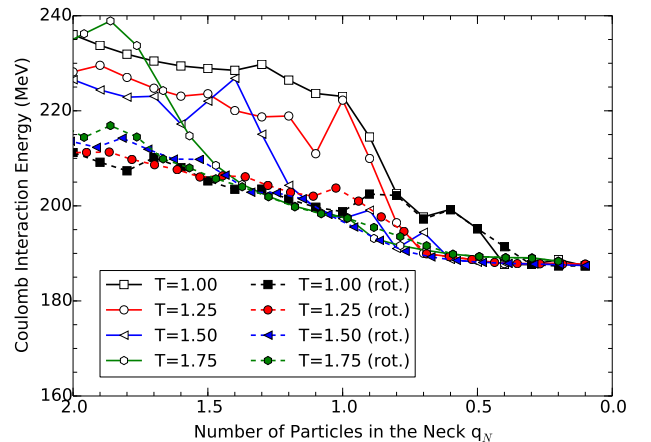


FIG. 12. (color online) Same as Fig. 11 in the higher temperature range  $1.00 \leq T \leq 1.75$  MeV.

Finally, figure 12 shows the evolution of the direct

Coulomb interaction energy along the  $\hat{Q}_N$  path at higher temperatures  $T \geq 1.00$  MeV. This corresponds to incident neutron energies larger than 25 MeV. In this regime, pairing correlations have vanished entirely. Quite surprisingly, the total Coulomb interaction energy is nearly constant at low  $q_N$  values, and this constant value is the same for all temperatures. Considering the large uncertainties of the current calculations, it is premature to draw definitive conclusions, but this point calls for further studies.

The calculations presented here are clearly schematic and have yet to reach the accuracy obtained from evaluations [74]. We recall that the goal of this paper is to set up a framework based on finite-temperature DFT that can be used in more systematic studies. In particular, it becomes clear from figures 9-12 that scission configurations must be identified from a PES that is fully continuous, which should remove some of the fluctuations observed here. This can be achieved by considering simultaneously all relevant collective variables, i.e., at least  $\hat{Q}_{20}$ ,  $\hat{Q}_{22}$ ,  $\hat{Q}_{30}$ ,  $\hat{Q}_{40}$  and  $\hat{Q}_N$ , together with the temperature. In order to compare theoretical predictions with experimental data, which is based on the average total kinetic energy, the local enlargement of the collective space should be repeated for all fragmentations observed in the  $^{239}\text{Pu}(n,f)$  reaction. Improvements on the quantum localization methods are also possible. Work along these lines is currently under way.

## V. CONCLUSIONS

One of the main challenges for a theory of induced fission is the need to accurately describe the (possibly high) excitation energy of the compound nucleus. In this paper, we have adopted the finite-temperature nuclear density formalism to describe neutron-induced fission:

- We have validated the nuclear DFT framework at finite-temperature for the description of induced fission. In particular, we have given a prescription to relate the excitation energy of the compound nucleus to the nuclear temperature of the FT-HFB theory. Following Ref. [25], we have confirmed the validity of the Maxwell relations of thermodynamics over the entire fission pathway, with the exception of the scission region (unless there are enough collective variables to make the potential energy surface continuous).
- We have quantified the effect of the incident neutron energy on the fission barriers of the compound nucleus  $^{240}\text{Pu}$ . In particular, we have found that fission barriers slightly increase in the energy range  $E_n = 0 - 5$  MeV; at higher neutron energies, the trend is reversed and fission barriers decrease monotonically. We stress that, in the energy range of interest in applications of induced fission, ( $E_n = 0 - 14$  MeV), the barriers are lower by at

most 15%. While this can have a significant impact on fission observables, in particular fission probabilities, the effect is not as dramatic as may have been expected from, e.g., studies of cold fusion in superheavy nuclei [24].

- We have given a microscopic foundation at  $T > 0$  of the central hypothesis of induced fission as a two-step process based on the decay of a compound nucleus. Indeed, we have confirmed that the coupling to the continuum induced by the finite temperature is negligible at least up to 50 MeV of excitation energy ( $T \approx 1.5$  MeV) and remain small even at larger excitation energies.
- We have generalized the quantum localization method of Ref. [72] to the case of the finite-temperature DFT, showing that the method remains applicable up to  $T \approx 1.5$  MeV. We have found that scission tends to occur at larger values of the number of particles in the neck as temperature increases.

In principle, the finite-temperature DFT framework should allow us to compute the excitation energy of the fragment in a fully microscopic way. There are, however, multiple caveats. First of all, we have seen that the position of the scission point changes with temperature. The charge and mass of the fission fragments also change: the evolution of a given fragment ( $Z, N$ ) as a function of the excitation energy of the compound nucleus can not be obtained from a single fission pathway only, but requires the full local scission hyper-surface. An additional difficulty is that both the charge and mass of the fragments are non-integer numbers, through both quantum and statistical fluctuations. Of course, we may perform HFB calculations for the fragments by imposing that  $\langle \hat{Z} \rangle$  and  $\langle \hat{N} \rangle$  take any value, including fractional ones, but it is not clear how accurate this approximation would be.

In this work, we have restricted ourselves to a static view of the fission process. A dynamical treatment of the process would certainly require an extension of the microscopic theory of collective inertia at finite temperature. This would allow both fully consistent computations of spontaneous fission half-lives in the commonly adopted WKB approximation and calculations of fission yields and energy distributions in the time dependent generator coordinate method such as in Refs. [34, 35, 75].

## ACKNOWLEDGMENTS

Stimulating discussions with W. Younes, D. Gogny, D. Regnier, and J. Randrup are very gratefully acknowledged. We are also thankful to W. Nazarewicz and J.C. Pei for useful comments. This work was partly performed under the auspices of the U.S. Department of Energy by Lawrence Livermore National Laboratory

under Contract DE-AC52-07NA27344. Funding was also provided by the U.S. Department of Energy Office of Science, Nuclear Physics Program pursuant to Contract DE-AC52-07NA27344 Clause B-9999, Clause H-9999, and the American Recovery and Reinvestment Act, Pub. L. 111-5. Computational resources were provided through an INCITE award “Computational Nu-

clear Structure” by the National Center for Computational Sciences (NCCS) and National Institute for Computational Sciences (NICS) at Oak Ridge National Laboratory, and through an award by the Livermore Computing Resource Center at Lawrence Livermore National Laboratory. Thanks are also due to the UK Engineering and Physical Sciences Research Council, under Grant EP/J013072/1.

- 
- [1] M. B. Chadwick, M. Herman, P. Obložinský, M. E. Dunn, Y. Danon, A. C. Kahler, D. L. Smith, B. Pritychenko, G. Arbanas, R. Arcilla, R. Brewer, D. A. Brown, R. Capote, A. D. Carlson, Y. S. Cho, H. Derrien, K. Guber, G. M. Hale, S. Hoblit, S. Holloway, T. D. Johnson, T. Kawano, B. C. Kiedrowski, H. Kim, S. Kunieda, N. M. Larson, L. Leal, J. P. Lestone, R. C. Little, E. A. McCutchan, R. E. MacFarlane, M. MacInnes, C. M. Mattoon, R. D. McKnight, S. F. Mughabghab, G. P. A. Nobre, G. Palmiotti, A. Palumbo, M. T. Pigni, V. G. Pronyaev, R. O. Sayer, A. A. Sonzogni, N. C. Summers, P. Talou, I. J. Thompson, A. Trkov, R. L. Vogt, S. C. van der Marck, A. Wallner, M. C. White, D. Wiarda, and P. G. Young, Nucl. Data Sheets Special Issue on ENDF/B-VII.1 Library, **112**, 2887 (2011).
- [2] B. Watt, Phys. Rev. **87**, 1037 (1952).
- [3] N. Bohr and J. A. Wheeler, Phys. Rev. **56**, 426 (1939).
- [4] A. Bohr and B. Mottelson, *Nuclear Structure*, Vol. II (Benjamin, New-York, 1975).
- [5] T. Duguet, M. Bender, K. Bennaceur, D. Lacroix, and T. Lesinski, Phys. Rev. C **79**, 044320 (2009).
- [6] D. Lacroix, T. Duguet, and M. Bender, Phys. Rev. C **79**, 044318 (2009).
- [7] M. Bender, K. Bennaceur, T. Duguet, P. H. Heenen, T. Lesinski, and J. Meyer, Phys. Rev. C **80**, 064302 (2009).
- [8] M. V. Stoitsov, J. Dobaczewski, R. Kirchner, W. Nazarewicz, and J. Terasaki, Phys. Rev. C **76**, 014308 (2007).
- [9] M. Anguiano, J. L. Egidio, and L. M. Robledo, Nucl. Phys. A **696**, 467 (2001).
- [10] R. Bernard, H. Goutte, D. Gogny, and W. Younes, Phys. Rev. C **84**, 044308 (2011).
- [11] R. Eschrig, *Fundamentals of Density Functional Theory* (Teubner, Leipzig, 1996).
- [12] R. Parr and W. Yang, *Density Functional Theory of Atoms and Molecules* (Oxford University Press, Oxford, 1989).
- [13] J.-P. Blaizot and G. Ripka, *Quantum Theory of Finite Systems* (The MIT Press, Cambridge, 1985).
- [14] J. des Cloizeaux, in *Many-Body Physics*, edited by C. DeWitt and R. Balian (Gordon and Breach, Science Publishers, Inc., 1968).
- [15] F. Garcias, M. Barranco, A. Faessler, and N. Ohtsuka, Z. Physik A **336**, 31 (1990).
- [16] F. Garcias, M. Barranco, J. Nemeth, C. Ngô, and X. Viñas, Nucl. Phys. A **495**, 169 (1989).
- [17] C. Guet, E. Strumberger, and M. Brack, Phys. Lett. B **205**, 427 (1988).
- [18] D. Dalili, J. Németh, and C. Ngô, Z. Physik A **321**, 335 (1985).
- [19] J. Nemeth, D. Dalili, and C. Ngô, Phys. Lett. B **154**, 11 (1985).
- [20] M. Diebel, K. Albrecht, and R. W. Hasse, Nucl. Phys. A **355**, 66 (1981).
- [21] J. Bartel, M. Brack, and M. Durand, Nucl. Phys. A **445**, 263 (1985).
- [22] M. Brack and P. Quentin, Phys. Lett. B **52**, 159 (1974).
- [23] J. McDonnell, N. Schunck, and W. Nazarewicz, in *Fission and Properties of Neutron-Rich Nuclei* (World Scientific, Sanibel Island, Florida, USA, 2013) p. 597.
- [24] J. A. Sheikh, W. Nazarewicz, and J. C. Pei, Phys. Rev. C **80**, 011302 (2009).
- [25] J.C. Pei, W. Nazarewicz, J.A. Sheikh, and A.K. Kerman, Phys. Rev. Lett. **102**, 192501 (2009).
- [26] S. Hilaire, M. Girod, S. Goriely, and A.J. Koning, Phys. Rev. C **86**, 064317 (2012).
- [27] J.L. Egidio, L.M. Robledo, and V. Martin, Phys. Rev. Lett. **85**, 26 (2000).
- [28] J. L. Egidio and P. Ring, J. Phys. G: Nucl. Part. Phys. **19**, 1 (1993).
- [29] J. L. Egidio, Phys. Rev. Lett. **61**, 767 (1988).
- [30] N. Schunck, J. D. McDonnell, J. Sarich, S. M. Wild, and D. Higdon, arXiv:1406.4383 (2014).
- [31] M. Bender, P. Heenen, and P. Reinhard, Rev. Mod. Phys. **75**, 121 (2003).
- [32] P. Ring and P. Schuck, *The Nuclear Many-Body Problem* (Springer-Verlag, 2000).
- [33] W. Younes and D. Gogny, *Fragment Yields Calculated in a Time-Dependent Microscopic Theory of Fission*, Tech. Rep. LLNL-TR-586678 (Lawrence Livermore National Laboratory (LLNL), Livermore, CA, 2012).
- [34] H. Goutte, J.F. Berger, P. Casoli, and D. Gogny, Phys. Rev. C **71**, 024316 (2005).
- [35] J. F. Berger, M. Girod, and D. Gogny, Nucl. Phys. A **502**, 85 (1989).
- [36] J. Randrup and P. Möller, Phys. Rev. Lett. **106**, 132503 (2011).
- [37] J. Randrup, P. Möller, and A. J. Sierk, Phys. Rev. C **84**, 034613 (2011).
- [38] L. Reichl, *A Modern Course in Statistical Physics* (John Wiley and Sons, Inc, 1988).
- [39] A. L. Goodman, Nucl. Phys. A **528**, 348 (1991).
- [40] L. G. Moretto, Nucl. Phys. A **182**, 641 (1972).
- [41] J. Dudek, B. Herskind, W. Nazarewicz, Z. Szymanski, and T. R. Werner, Phys. Rev. C **38**, 940 (1988).
- [42] N. Schunck, J. Dudek, and B. Herskind, Phys. Rev. C **75**, 054304 (2007).
- [43] J. Randrup and P. Möller, Phys. Rev. C **88**, 064606 (2013).
- [44] K. Dietrich, J. Niez, and J. Berger, Nucl. Phys. A **832**, 249 (2010).

- [45] H. C. Lee and S. DasGupta, *Phys. Rev. C* **19**, 2369 (1979).
- [46] A. L. Goodman, *Nucl. Phys. A* **352**, 30 (1981).
- [47] K. Tanabe, K. Sugawara-Tanabe, and H. J. Mang, *Nucl. Phys. A* **357**, 20 (1981).
- [48] V. Martin, J.L. Egido, and L.M. Robledo, *Phys. Rev. C* **68**, 034327 (2003).
- [49] J. Dobaczewski, H. Flocard, and J. Treiner, *Nucl. Phys. A* **422**, 103 (1984).
- [50] J. Dobaczewski and J. Dudek, *Acta Phys. Pol. B* **27**, 45 (1996).
- [51] P. Bonche, S. Levit, and D. Vautherin, *Nucl. Phys. A* **436**, 265 (1985).
- [52] P. Bonche, S. Levit, and D. Vautherin, *Nucl. Phys. A* **427**, 278 (1984).
- [53] S. Levit and Y. Alhassid, *Nucl. Phys. A* **413**, 439 (1984).
- [54] J. Bartel, P. Quentin, M. Brack, C. Guet, and H. H\aaakansson, *Nucl. Phys. A* **386**, 79 (1982).
- [55] J. Dechargé and D. Gogny, *Phys. Rev. C* **21**, 1568 (1980).
- [56] W. Younes and D. Gogny, in *AIP Conference Proceedings*, Vol. 1175 (AIP Publishing, 2009) p. 3.
- [57] N. Schunck, A. Baran, M. Kortelainen, J. McDonnell, J. Moré, W. Nazarewicz, J. Pei, J. Sarich, J. Sheikh, and A. Staszczak, “Computing heavy elements,” (2011).
- [58] M. Stoitsov, N. Schunck, M. Kortelainen, N. Michel, H. Nam, E. Olsen, J. Sarich, and S. Wild, *Comput. Phys. Comm.* **184**, 1592 (2013).
- [59] N. Schunck, *Acta Phys. Pol. B* **44**, 263 (2013).
- [60] N. Schunck, *J. Phys.: Conf. Ser.* **436**, 012058 (2013).
- [61] M. Baranger and M. Veneroni, *Ann. Phys.* **114**, 123 (1978).
- [62] L. Landau and E. Lifshitz, *Statistical Physics, Part* (Pergamon Press Ltd., Oxford, 1980).
- [63] T. Dittrich, P. Hänggi, G.-L. Ingold, B. Kramer, G. Schön, and W. Zwerger, *Quantum Transport and Dissipation* (Wiley-VCH, Weinheim, 1998).
- [64] M. Razavy, *Classical and Quantum Dissipative Systems* (Imperial College Press, 2005).
- [65] A. V. Ignatyuk, I. N. Mikhailov, L. H. Molina, R. G. Nazmitdinov, and K. Pomorsky, *Nucl. Phys. A* **346**, 191 (1980).
- [66] G. Sauer, H. Chandra, and U. Mosel, *Nucl. Phys. A* **264**, 221 (1976).
- [67] U. Mosel, P. Zint, and K. H. Passler, *Nucl. Phys. A* **236**, 252 (1974).
- [68] R. W. Hasse and W. Stocker, *Phys. Lett. B* **44**, 26 (1973).
- [69] V. Martin and L. M. Robledo, *Int. J. Mod. Phys. E* **18**, 861 (2009).
- [70] M. Brack, J. Damgaard, A. S. Jensen, H. C. Pauli, V. M. Strutinsky, and C. Y. Wong, *Rev. Mod. Phys.* **44**, 320 (1972).
- [71] D. Duke, H. Carr, A. Knoll, N. Schunck, H. A. Nam, and A. Staszczak, *IEEE Trans. Vis. Comp. Graph.* **18**, 2033 (2012).
- [72] W. Younes and D. Gogny, *Phys. Rev. Lett.* **107**, 132501 (2011).
- [73] J. Dobaczewski and P. Olbratowski, *Comput. Phys. Comm.* **158**, 158 (2004).
- [74] D. G. Madland, *Nucl. Phys. A* **772**, 113 (2006).
- [75] H. Goutte, P. Casoli, and J. F. Berger, *Nucl. Phys. A* **734**, 217 (2004).